HAL
archives-ouvertes.fr

Transient geotherms in Archean continental lithosphere: New constraints on thickness and heat production of the subcontinental lithospheric mantle

Christophe Michaut, Claude Jaupart, D. R. Bell

▶ To cite this version:

Christophe Michaut, Claude Jaupart, D. R. Bell. Transient geotherms in Archean continental lithosphere: New constraints on thickness and heat production of the subcontinental lithospheric mantle. Journal of Geophysical Research : Solid Earth, American Geophysical Union, 2007, 10.1029/2006JB004464 . insu-01289160

HAL Id: insu-01289160
https://hal-insu.archives-ouvertes.fr/insu-01289160

Submitted on 16 Mar 2016

HAL is a multi-disciplinary open access archive for the deposit and dissemination of scientific research documents, whether they are published or not. The documents may come from teaching and research institutions in France or abroad, or from public or private research centers.

L'archive ouverte pluridisciplinaire **HAL**, est destinée au dépôt et à la diffusion de documents scientifiques de niveau recherche, publiés ou non, émanant des établissements d'enseignement et de recherche français ou étrangers, des laboratoires publics ou privés.

Transient geotherms in Archean continental lithosphere: New constraints on thickness and heat production of the subcontinental lithospheric mantle

C. Michaut,[1,3] C. Jaupart,[1] and D. R. Bell[2]

Received 24 April 2006; revised 16 December 2006; accepted 28 December 2006; published 25 April 2007.

[1] Because of its large thickness and thermal relaxation time, Archean lithosphere cannot be in thermal equilibrium with the instantaneous rate of heat production in the lithospheric mantle and heat supplied to its base. Comparison of xenolith (*P*,*T*) data with time-dependent thermal models allows constraints on lithosphere thickness, in situ heat production in the lithospheric mantle and time changes of basal heat flux. In this paper, the lithosphere is defined as the rigid part of the thermal boundary layer where heat transport occurs by conduction only. A Monte Carlo procedure is used to determine the full range of thermal models consistent with xenolith (*P*,*T*) arrays from Newlands and Finsch orangeites, Kaapvaal craton, South Africa. These xenolith suites from an early phase of kimberlite magmatism in the Kaapvaal record thermal conditions in unperturbed lithosphere. Together with constraints on surface heat flow and crustal heat production, these data require the lithosphere thickness to be between 200 and 270 km, with most values between 210 and 250 km. Additional constraints, including the condition that lithospheric temperatures have remained below the solidus, estimates of the cooling rate in mantle xenoliths, and the depth extent of seismic anomalies beneath cratons tighten the solution range. Present-day values of basal heat flow and heat production in the Kaapvaal lithospheric mantle lie between 12–16 mW m^{-2} and 0–0.02 μW m^{-3} respectively. At 240-km depth, lithospheric material undergoes secular cooling at a rate of 40 to 110 K/Ga due solely to in situ radioactive decay. Changes of basal heat flow must be less than 5% per Ga, suggesting that thermal conditions in the underlying mantle have not changed much since the Archean.

Citation: Michaut, C., C. Jaupart, and D. R. Bell (2007), Transient geotherms in Archean continental lithosphere: New constraints on thickness and heat production of the subcontinental lithospheric mantle, *J. Geophys. Res.*, *112*, B04408, doi:10.1029/2006JB004464.

1. Introduction

[2] The characteristic time for heat diffusion in a 250-km-thick lithosphere, given by $\frac{H^2}{\kappa}$, where H is thickness, is equal to 2 Ga, which implies that the continental lithosphere records low-frequency thermal variations. In particular, this timescale is comparable to the half-lives of the four main heat-producing isotopes, ^{238}U, ^{235}U, ^{232}Th, and ^{40}K. For typical values of isotopic ratios in mantle rocks, radiogenic heat production has decreased by a factor of 2 in the last 2.75 Ga. In this case, as shown by *Michaut and Jaupart* [2004], a continental root is not in thermal equilibrium with the instantaneous rate of heat production and its geotherm is sensitive to the decay of its heat-producing elements. In addition, continental lithosphere drifts on top of the convective mantle, which undergoes secular cooling. This is responsible for yet another thermal transient which may affect continental geotherms. From laboratory experiments and simple theory, *Guillou and Jaupart* [1995] derived the following estimate for the characteristic time τ_s of thermal transients beneath a lid:

$$\tau_s \approx 10 \frac{d^2}{\kappa} Ra^{-1/3} \quad (1)$$

where Ra is a Rayleigh number for the convective system. For example, τ_s takes a value of about 2.7 Ga for d = 2000 km, $\kappa = 10^{-6}$ m^2 s^{-1}, and $Ra = 10^8$, which is again very close to the characteristic time for diffusion in thick lithosphere. We must therefore conclude that the continental lithosphere evolves in a transient thermal regime which affects the shape of its geotherm.

[3] Accounting for transient thermal effects within thick continental lithosphere affects the interpretation of (*P*,*T*) data derived from thermodynamic studies of mantle xenoliths [*Michaut and Jaupart*, 2004]. Thus, for example, the basal heat flux sustained by the underlying convecting mantle takes smaller values than in steady state calculations. Another consequence is perhaps more interesting and deals

[1]Laboratoire de Dynamique des Systemes Geologiques, Institut de Physique du Globe de Paris, Paris, France.
[2]Department of Chemistry and Biochemistry, and School of Earth and Space Exploration, Arizona State University, Tempe, Arizona, USA.
[3]Now at Department of Geology and Geophysics, Yale Univesity, New Haven, Connecticut, USA.

Copyright 2007 by the American Geophysical Union.
0148-0227/07/2006JB004464$09.00

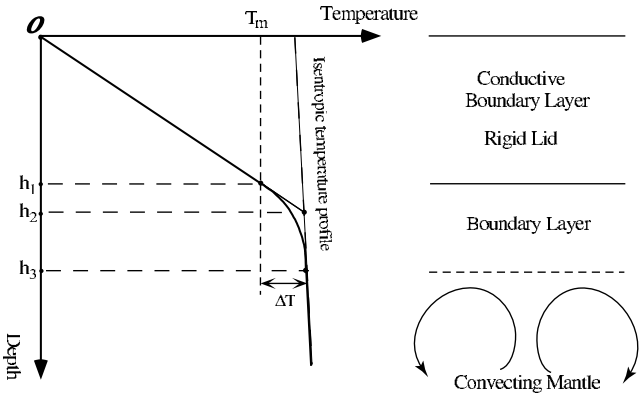

Figure 1. Thermal structure of the continental lithosphere and underlying mantle. The thickness of continental lithosphere can be defined in three different ways. The thickness of the purely conductive boundary layer, or rigid lid, is h_1, which is the definition used here. h_2 is determined from the intersection of the conductive temperature profile and an assumed isentropic temperature profile in the convecting mantle. h_3 is the total thickness of the thermal boundary layer, defined as the layer where temperature departs significantly from the isentropic profile. Seismological studies provide constraints on h_2 or h_3.

with the lithosphere thickness itself. Different geophysical methods have been used to determine the lithosphere thickness and have led to contrasting results. Part of the problem is simply that each method deals with a different definition, as sketched in Figure 1. Seismological estimates of Archean lithosphere thickness are in the range of 250–400 km [*Jordan*, 1975; *Gung et al.*, 2003], significantly larger than estimates from the downward extrapolation of geotherms or from fits to (*P*,*T*) xenolith data, which are between 200 and 250 km [*Rudnick and Nyblade*, 1999]. This difference is consistent with the structure of the thermal boundary layer sketched in Figure 1. As shown by Figure 1, however, neither method can constrain the thickness of the rigid lid, which corresponds to the purely conductive part of the thermal boundary layer. Yet, it is precisely that part which is really useful in geological studies because, for example, it records tectonic deformation and thermal transients following stretching and thickening. One additional problem involves the difficulty in evaluating the uncertainties in thickness determinations. For example, geotherms deduced from heat flow or xenolith (*P*,*T*) data are extended to a hypothetical isentropic temperature profile which is supposed to characterize the convecting mantle below the continental lid. This procedure relies on an estimate of the potential temperature for the well-mixed mantle. As many studies have shown, however, the subcontinental convective mantle is probably not at the same potential temperature than neighboring oceanic regions. Thus, there is no straightforward way to determine the bottom of the thermal boundary layer beneath continents. Here we shall focus on precisely the rigid part of the boundary layer where heat is transported by conduction only (Figure 1). The same definition is used when studying thermal transients such as the subsidence of intracratonic basins [*Kaminski and Jaupart*, 2000]. Cratonic lithosphere is highly depleted in fertile components and intrinsically buoyant with respect to undepleted mantle, which makes it stable against convective overturn [*Boyd and McCallister*, 1976; *Jordan*, 1988]. It is a chemical boundary layer and hence may be an important repository of trace elements. Here what matters again is that part of the thermal boundary layer which does not get involved in convective overturn, such that heat transport proceeds by conduction only.

[4] In this study, we account for transient thermal effects due to radioactive decay and to variations of heat supply at the base of the lithosphere in an analysis of (*P*,*T*) data from South African mantle xenoliths. By construction, therefore, this study focuses on the conductive part of the lithosphere and leads to constraints on its thickness. We shall emphasize that, for given (*P*,*T*) data, thickness estimates depend on the amounts of radioelements in the lithospheric mantle, which provides a link between geophysical and geochemical issues. We use the large data set of xenolith *P*,*T* array and surface heat flow determinations available for the Archean Kaapvaal craton, South Africa. We have selected xenoliths erupted in the Newlands (114 Ma) and Finsch (118 Ma) orangeites, which predate the main kimberlite pulse at 90–70 Ma. Those samples provide the best long-term estimate of the cratonic geotherm unperturbed by prior kimberlite magmatism. We systematically explore the range of values for all the parameters of the thermal model that allow a good fit to these data. More specifically, the parameter space explored includes heat production rates in the upper crust, lower crust, and lithospheric mantle, the lithosphere thickness, as well as the heat flux at the base of the lithosphere and how it varies through time. Ranges of possible values for the lithosphere thickness and heat generation in the lithospheric mantle are discussed. Secular changes of basal temperature and basal heat flux are evaluated.

2. Method

2.1. Thermal Model

[5] Thermal evolution of thick lithosphere proceeds in two stages. In an initial transient, the lithosphere undergoes thermal relaxation from its initial, and poorly known, structure. The second transient stage is such that lithospheric temperatures evolve solely because of the rundown of radioactive elements and changes of the basal heat flow, independently of the initial thermal structure. For Archean lithosphere with an age of about 3 Ga, i.e., larger than the diffusive timescale, the initial thermal relaxation has proceeded to completion. This has been verified using a full transient calculation presented in Appendices A and B.

[6] We are interested in the thermal structure of stable Archean lithosphere and assume that lithosphere thickness remains constant. In the reference frame of the continent, heat transfer occurs by conduction in the vertical direction, save for shallow crustal environments with large lateral variations of radiogenic heat production. In this reference frame, convective processes lead to relatively short timescale fluctuations in the thermal basal condition. Advection of heat due to stretching and thickening of the whole lithosphere is also neglected because the induced transient thermal evolution is similar to the initial transient following continental formation, with a thermal relaxation of less than ≈500 Ma (see Appendix B). Crustal stretching and thickening are more common, but the induced thermal transients

are even more short-lived because they occur close to the surface.

[7] The equation for vertical diffusive heat transport in the lithosphere is:

$$\frac{\partial T}{\partial t} = \kappa \frac{\partial^2 T}{\partial z^2} + \frac{A_i(t)}{\rho C_P} \tag{2}$$

where T is the temperature, t is the function of time, z is the depth, and κ is the thermal diffusivity. C_P, which is the heat capacity, and ρ, which is the density, are taken to be constant in the whole lithosphere. $A_i(t)$ represents in situ heat production. We do not account for the temperature dependence of conductivity, which has only minor effects on the end results, as discussed in Appendix A. For simplicity, we take a single value for thermal diffusivity in both crust and mantle. Crustal rocks have both lower conductivity and lower density than mantle rocks, such that changes of thermal diffusivity are very small. These simplifications allow a fully analytical solution for the temperature field detailed in Appendix C.

[8] The model differs from the preceding paper [*Michaut and Jaupart*, 2004] in that the lithosphere is composed of three reservoirs, instead of two. We found it necessary to distinguish between an upper crust enriched in radioactive elements and a depleted lower crust. The third reservoir is the lithospheric mantle. As discussed in Appendix D, we have attempted to separate the lithospheric mantle into two reservoirs with different heat generation rates, but the data do not possess sufficient resolving power. With respect to our earlier study, one significant difference is a dampening of transient effects due to crustal heat production because heat produced in the upper crust is rapidly transported to the surface. Other differences are the use of several independent constraints and allowance for time-dependent basal heat flux.

[9] Each reservoir contains different amounts of radiogenic nuclides ^{238}U, ^{235}U, ^{232}Th, and ^{40}K. Time dependence of heat generation is approximated by a single exponential function:

$$A_i(t) = A_{i0} \exp^{-\frac{t-t_0}{\tau_r}} \tag{3}$$

where A_{i0} is the radioactive heat production at t_0 and indices $i = c$, s, and m stand for upper crust, lower crust, and lithospheric mantle respectively. τ_r is the weighted average radioactive decay constant, which was set equal to 3.96 Ga, corresponding to a half-life of 2.75 Ga. We assume that all reservoirs have the same elemental ratios Th/U and K/U and hence the same decay constant.

[10] Mantle convection supplies heat to the base of the lithosphere. For our present purposes, the most appropriate boundary condition is one of heat flux so that we may solve for the basal temperature, which allows a useful comparison with independent estimates of the rate of secular cooling of our planet. Specifying the basal temperature is possible, of course, but leads to results that are mathematically equivalent. For simplicity, the basal heat flow, noted $Q_b(t)$, is expressed as an exponential function of time with decay constant τ_s:

$$Q_b(t) = Q_{b0} \exp^{-\frac{t-t_0}{\tau_s}} \tag{4}$$

where Q_{b0} is the basal heat flow at t_0. The advantage of such a function is that it allows a straightforward analytical solution. In this framework, we are focusing on long-term changes of heat supply at the base of the lithosphere and do not consider shorter transients associated with mantle plumes for example.

2.2. Transient Temperature Profiles

[11] Because of the linearity of the heat equation, the instantaneous vertical temperature profile is the sum of four components (upper crust, lower crust, lithospheric mantle, and basal heat flow):

$$T(z,t) = T_c(z,t) + T_s(z,t) + T_m(z,t) + T_b(z,t) \tag{5}$$

where the contribution of each transient heat source is considered separately. Heat production and the basal heat flow are associated with two different decay constants, such that:

$$T_i(z,t) = Z_i(z) e^{-\frac{t-t_0}{\tau_r}}, \quad i = c,s,m \tag{6}$$

$$T_b(z,t) = Z_b(z) e^{-\frac{t-t_0}{\tau_s}} \tag{7}$$

where subscripts c, s, m, and b refer to the component upper crust, lower crust, lithospheric mantle, and basal heat flow respectively. Functions $Z_i(z)$ are easily determined from the heat equation, applying continuity of temperature and heat flux at the interfaces between the upper and lower crust and between the lower crust and the lithospheric mantle (see the work of *Michaut and Jaupart* [2004] and Appendix C for more details). For the sake of example, Figure 2 shows results for a specific choice of parameters. Both radioactive decay and secular cooling of the underlying mantle act to increase the curvature of the instantaneous vertical temperature profile with respect to a steady state profile with the same parameter values. For a constant conductivity, curvature increases with depth because heat gets transported to the surface with decreasing efficiency.

[12] Instantaneous cooling rates are easily calculated for each component as a function of time and depth. Cooling due to radioactive or basal heat flow decay is respectively:

$$\left[-\frac{\partial T}{\partial t}\right]_r (z,t) = \frac{T_c(z,t) + T_s(z,t) + T_m(z,t)}{\tau_r} \tag{8}$$

$$\left[-\frac{\partial T}{\partial t}\right]_s (z,t) = \frac{T_b(z,t)}{\tau_s} \tag{9}$$

The instantaneous temperature profile depends thus on six parameters: A_{c0}, A_{s0}, A_{m0}, Q_{b0}, τ_s, H, corresponding to three present-day values for heat production in the three reservoirs and three parameters for the basal boundary condition, lithosphere thickness H, the present-day value and decay time of the basal heat flow. This defines the parameter space of the problem, which was explored with a Monte Carlo method. This method employs a random number generator to generate random models. The observables are calculated for each model and compared with

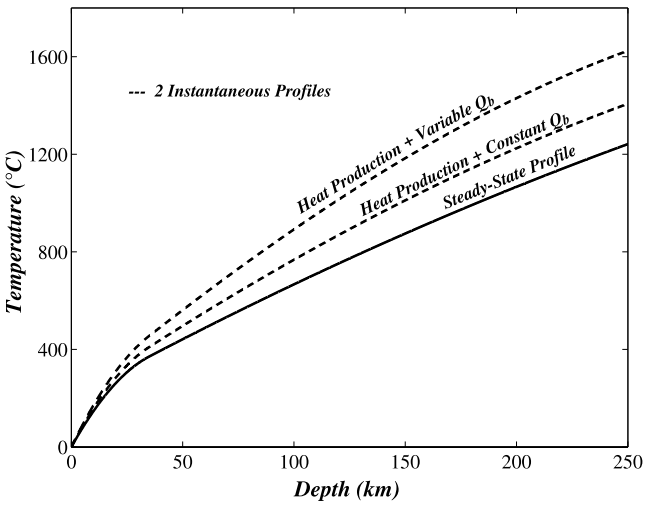

Figure 2. Two instantaneous temperature profiles (dashed lines) emphasizing transient effects in thick lithosphere, compared with the predictions of a steady state model (solid line) with the same parameter values. For the lower dashed curve, calculations account for radioactive decay only and the heat flow at the base of the lithosphere is kept at a constant value. For the upper dashed curve, calculations account for the decay of both radioactive heat sources and basal heat flow. Transient profiles exhibit an important curvature and are hotter than the steady state profile derived for the same set of parameters because of inefficient heat transport through a thick conductive lid. Values for the various parameters used are as follows: τ_s = 3 Ga (τ_s is the logarithmic decrement for an exponentially decreasing basal heat flow), A_{c0} = 1.0 μW m^{-3}, A_{s0} = 1.0 μW m^{-3}, A_{m0} = 0.02 μW m^{-3}, Q_{b0} = 10.0 mW m^{-2}, and H = 250 km.

real data. Random model parameters are generated within a range of values, discussed below, estimated from other geochemical, seismological, and thermal studies (see Table 1).

3. The Kaapvaal Craton

[13] The Kaapvaal craton, South Africa offers the most comprehensive data set, which provides strong constraints on the acceptable model space.

3.1. Model Parameters and Model Space

[14] Estimates of continental lithosphere thickness vary significantly, from as much as 400 to about 200 km or less [*Jordan*, 1975; *Jaupart and Mareschal*, 1999; *Priestley*, 1999]. Differences come from intrinsic uncertainties in the data as well as from different definitions for the lithosphere (Figure 1). For instance, *S-P* traveltime residuals and receiver function images consistently show that the 410-km discontinuity is not deflected beneath the Kaapvaal root [*Niu et al.*, 2004]. This observation, together with geodynamical modeling, constrains the depth of this root to lie in the range of 160 to 370 km. *P* and *S* wave seismic tomography suggests a minimum depth in places of about 250 km as well as a substantial degree of lateral variation [*James et al.*, 2001]. In their thermal study, *Rudnick and Nyblade* [1999] calculate a posteriori a thickness of about 200 to 250 km for this craton, using the assumption that the basal temperature lies along an isentropic temperature profile. Petrological studies suggest a range between 160 and 220 km [*Boyd and Gurney*, 1986; *Griffin et al.*, 2003]. We discuss these discrepancies later in this paper. In our calculations, values of H are generated within a range of 160 to 400 km, in agreement with the study of *Niu et al.* [2004].

[15] Radiogenic heat production in the upper crust can be measured directly and is relatively well known. It is now determined routinely in conjunction with heat flow measurements [*Jaupart et al.*, 1998]. Thus, the range of acceptable values for A_{c0} is rather small and will be used more as an additional constraint than as a domain to explore. In the center of the Kaapvaal craton, the Witwatersrand basin, including the Vredefort structure, has been extensively studied for its heat flow and heat production characteristics [*Nicolaysen et al.*, 1981; *Jones*, 1988]. *Nicolaysen et al.* [1981] measured heat produced in each lithological unit of the Vredefort basement and estimated that crustal heat production contributes to about 29 to 34 mW m^{-2} of the total heat flow for a 36-km-thick crust. A 6-km-thick sequence of highly radioactive sedimentary rocks contributes about 7.5 mW m^{-2}. To define an average range of values for upper and lower crustal heat production for the entire Kaapvaal craton, we do not consider this local contribution. Beneath this thick sedimentary sequence, the average heat production is 1.8 μW m^{-3} in the 7-km-thick upper portion of the Vredefort basement and 1.0 μW m^{-3} in the 7-km-thick lower portion of it. Thus, for an upper crust

Table 1. Parameters, Data and Constraints

Parameters	Symbol	Value
Crustal Thermal Conductivity	k_c	2.54 W m^{-1} K^{-1}
Mantle Thermal Conductivity	k_m	3.00 W m^{-1} K^{-1}
Thermal Diffusivity	κ	0.76 × 10^{-6} m^2 s^{-1}
Heat Capacity	C_P	1200 J K^{-1} kg^{-1}
Crustal Density	ρ_c	2800 kg m^{-3}
Mantle Density	ρ_m	3300 kg m^{-3}
Characteristic Time of Radioactive Decay	τ_r	3.96 Ga
Upper Crust Thickness	s	10 km
Crust Thickness	d	35 km
Model Parameters	**Symbol**	**A Priori Range of Values**
Upper Crust Heat Production	A_{c0}	1.40–1.70 μW m^{-3}
Lower Crust Heat Production	A_{s0}	0.10–0.60 μW m^{-3}
Mantle Heat Production	A_{m0}	0–0.06 μW m^{-3}
Lithosphere Thickness	H	160–400 km
Basal Heat Flow	Q_{b0}	8–20 mW m^{-2}
Characteristic Time of Basal Heat Flow Decay	τ_s	$\left(\frac{2}{\pi}\right)^2 \frac{H^2}{\kappa}$ – 62 Ga
Calculated Data	**Symbol**	**Acceptable Range of Values**
Temperature at 3.6 Gpa	$T_{3.6}$	770–880°C
Temperature at 4.1 Gpa	$T_{4.1}$	840–950°C
Temperature at 4.6 Gpa	$T_{4.6}$	900–1080°C
Temperature at 5.9 Gpa	$T_{5.9}$	1170–1270°C
First Set of Constraints		
Surface Heat Flow	Q_s	40–46 mW m^{-2}
Temperature at $z = H, t = t_0$	T_b	1250–1550°C
Second Set of Constraints		
Lithosphere Thickness	H	>220 km
Temperature at $z = H, t$ = 2.5 Ga	$T_{H,2.5\ Ga}$	$<T_{solidus}$
Cooling Rates	$\frac{dT}{dt}_{4.0-5.0Gpa,t_0}$	40–110 K/Ga

of thickness 10 km, heat production is about $A_{c0} \approx \frac{1.8 \times 7 + 1.0 \times 3}{10} \approx 1.6$; we shall allow it to vary between 1.4 to 1.7 μW m^{-3}.

[16] Lower crustal heat production A_{s0} is estimated using the contribution of crustal heat production in the heat flow and crustal thickness $d = 35$ km; it is taken to be in the range of 0.1 to 0.6 μW m^{-3}. Bulk crustal heat production is thus between 0.47 and 0.91 μW m^{-3}, consistent with independent estimates in Archean cratons [*Pinet and Jaupart*, 1987; *McLennan and Taylor*, 1996; *Rudnick et al.*, 1998].

[17] Heat production in the lithospheric mantle remains poorly known in all cratons. For instance, measurements of heat-producing elements in kimberlite-hosted peridotite xenoliths from the Slave craton, Canada, yield high estimates of mantle heat production, from 0.09 to 0.46 μW m^{-3} [*Russell and Kopylova*, 1999]. However, the temperature profile given by xenolith (P,T) data in this region implies that mantle heat production must be less than 0.088 μW m^{-3} [*Russell and Kopylova*, 1999]. Theoretical thermal models for other cratons do not agree with the high values that are measured in kimberlite-hosted xenoliths and support much lower values, between 0 and 0.04 μW m^{-3} [*Rudnick et al.*, 1998; *Rudnick and Nyblade*, 1999]. Heat flow data do not allow heat production rates that are larger than 0.08 μW m^{-3} in the lithospheric mantle [*Jaupart and Mareschal*, 1999]. Using appropriate values for the ratios K/U and K/Th, mean and median values of K content in on-craton peridotites give estimates of heat production between 0.019 and 0.104 μWm^{-3} [*Rudnick et al.*, 1998]. A number of metasomatic processes can enhance heat-producing element (HPE) contents of cratonic xenoliths, which can explain the discrepancies between theory and measurements. Metasomatic minerals that contain HPE, such as phlogopite and clinopyroxene, may be concentrated around areas of alkaline magmatic activity. This is especially evident in the case of some kimberlites. In addition, >90% of the incompatible element budget of many cratonic xenoliths which erupted in kimberlites resides on fractures and grain boundaries [*Grégoire et al.*, 2003] and may have been introduced during transport. These factors suggest that the observed HPE concentrations in kimberlite-hosted xenoliths have been present in xenoliths on a trivially short timescale compared with that of conductive equilibration of the lithosphere and are unrepresentative of long-term HPE concentrations. Peridotite xenoliths carried in alkali basalt are apparently less affected by such processes and seem to provide a better estimate of the heat produced in the mantle, about 0.02 to 0.03 μW m^{-3} [*Rudnick et al.*, 1998]. We thus consider values for present-day lithospheric mantle heat production between 0 and 0.06 μW m^{-3}.

[18] By removing local crustal heat production from surface heat flow, *Jaupart and Mareschal* [1999] estimated a Moho heat flow between 10 and 15 mW m^{-2} in eastern Canada, and *Jones* [1988] calculated a value of about 17 mW m^{-2} for the Kaapvaal craton, South Africa. We have seen that the maximum values for the bulk crustal heat production can be estimated at 0.91 μW m^{-3}. For a low surface heat flow of 40 mW m^{-2}, this leads to a lower limit of 8 mW m^{-2} for the mantle heat flow. The lowest surface heat flow measured in South Africa is 20 mW m^{-2} in Tanzania [*Nyblade et al.*, 1990] which provides an upper limit for the basal heat flow. A range from 8 to 20 mW m^{-2} for the basal heat flow is similar to the one used in the thermal study of *Rudnick and Nyblade* [1999] (8 to 21 mW m^{-2}).

[19] In the resolution of equation (2), the temporal period τ_s characteristic of basal heat flow variations translates into a spatial period appearing in the trigonometric terms of function $Z_b(z)$ equal to $2\pi(\tau_s\kappa)^{1/2}$. The lowest value for τ_s we consider corresponds to a spatial period equal to four times the thickness of the lithosphere, which amounts to: $\tau_s > \left(\frac{2}{\pi}\right)^2 \frac{H^2}{\kappa}$. For a 160-km-thick lithosphere, the smallest half-period of basal heat flow decay, such that heat flow decreases by a factor of 2, is thus 0.3 Ga, whereas for a 300-km-thick lithosphere it is 1.0 Ga. Fluctuations with shorter periods do not correspond to secular cooling conditions and reflect transient convective phenomena. They are not considered here and would not be handled accurately with the analytical solutions of Appendix C. The upper limit for τ_s is taken to be ~62 Ga, which effectively corresponds to a basal heat flow that remains constant.

3.2. (P,T) Data

[20] Mathematically, solutions are accepted with equal weight if calculated values fall within the ranges that were set a priori as explained above. The challenge is to assign an acceptable range of values for temperature at a given pressure that is consistent with xenolith data. Interpretation of (P,T) data from kimberlite-hosted xenoliths of the Kaapvaal craton has been controversial. Values derived from the thermobarometry method of *Brey and Kohler* [1990] indicate a relatively linear array for all xenolith types, including those of fertile chemical composition and deformed texture previously interpreted as being affected both chemically and thermally by melt-related metasomatism [*Gurney and Harte*, 1980; *Hops et al.*, 1989]. The linearity of the array encourages the simple, steady state interpretation with attendant estimates of lithospheric thickness [*Rudnick and Nyblade*, 1999]. This linearity is removed when other thermobarometers [*Taylor*, 1998] are applied, but there is at present no conclusive way to tell which thermobarometer method is most accurate for the high-temperature suite. Despite considerable efforts at thermobarometer calibration [*Smith*, 1999], the effects of minor components, for example, Ti [*Carswell*, 1991] or Fe^{3+} [*Canil and O'Neill*, 1996], on calculated pressure remain poorly understood.

[21] The dynamic aspects of Kaapvaal thermal and chemical evolution are apparent when xenolith data from orangeites and kimberlites of different ages are compared [*Bell*, 2002; *Bell et al.*, 2003; *Griffin et al.*, 2003; *Schmitz and Bowring*, 2003]. These studies conclude that temperature in the mantle of southern Africa increased in the tens of Ma preceding eruption of the main kimberlite pulse at 90–70 Ma. Therefore the best long-term estimates of the cratonic geotherm derive from xenoliths erupted in orangeites at 200–110 Ma. We therefore use a (P,T) data set from the Newlands and Finsch orangeites to constrain our set of permissible geotherm solutions [*Skinner*, 1989; *Bell*, 2002].

[22] For the Newlands data set, the agreement between different thermobarometry methods is good, which is not all that surprising given that the xenoliths of this suite do not contain highly fertile (Fe- and Ti-rich) minerals. Unfortunately, the data space cannot be constrained by this suite alone because the pressure range extends only to 5.3 GPa.

In order to better restrict the shape of the geotherm and derive new constraints for the thermal structure of the lithosphere from the curvature of the temperature profile, we have to add data coming from greater depth. We choose the Finsch data set because of the arguments listed above. The Finsch peridotites span a range of compositions from depleted to fertile, but all derive from a relatively restricted temperature and depth range. Because of the chemical complexity, the thermobarometry results differ more between methods than for the Newlands suite. These xenoliths may be thermally perturbed, but indicate temperatures about 100 K lower than xenoliths of corresponding depth from other Kaapvaal craton kimberlites [*Bell et al.*, 2003]. They therefore give an upper bound for the temperature at their depth of origin.

[23] For the purposes of consistency with previous studies, we use (*P*,*T*) data computed by the method of *Brey and Kohler* [1990] only. Its standard deviation is 2.2 kbar, i.e., about 7 km, at a given temperature, and 15°C at a fixed pressure [*Brey and Kohler*, 1990]. Using a thermal gradient of 4°C/km, this corresponds to an error in temperature of about 30°C. Thus, at a given pressure the total amplitude of the error is $(30 + 15) \times 2 = 90$°C. This error estimate derived from variations in the experimental calibration is likely to underestimate the total uncertainty for individual points because it does not consider possible systematic errors caused by compositional corrections. For the Newlands suite, however, such uncertainties are minimized.

[24] In effect the uncertainty in temperature at a given depth is less than the theoretical uncertainty of the thermobarometer because multiple (*P*,*T*) points constrain the geotherm. We use the following procedure to arrive at a more realistic estimate of temperature uncertainty. At a given pressure P_c, we determine the lower limit T_{inf} by determining the mean temperature T_m at $P_{inf} = P_c - \sigma_P$ and subtracting the standard deviation in temperature σ_T.

$$T_m = \frac{\sum_{i=1}^{n} T_i}{n} \tag{10}$$

$$\sigma_T = \frac{\sum_{i=1}^{n} |T_i - T_m|}{n} \tag{11}$$

where n is the number of xenolith (*P*,*T*) measurements between $P_{inf} - \sigma_P$ and $P_{inf} + \sigma_P$, and T_i is one of these measured temperatures. The upper limit is calculated reversely by determining the mean temperature T_m at $P_{sup} = P_c + \sigma_P$ and adding the standard deviation σ_T, calculated between $P_{sup} - \sigma_P$ and $P_{sup} + \sigma_P$. If the number of measurements is not sufficient to determine correctly this lower or upper limit, we used the lowest or highest temperature measured in the range $P_{inf} \pm \sigma_P$ or $P_{sup} \pm \sigma_P$ respectively. For these calculations, we used $\sigma_P = 2.5$ kbar. In order to take into account a maximum of measurements, we compare calculated temperatures to the acceptable range defined above at four different pressures: 3.6, 4.1, 4.6 and 5.9 GPa (Table 1 and Figure 3). Because of the data uncertainties, adding temperature values at other depths does not improve the solutions.

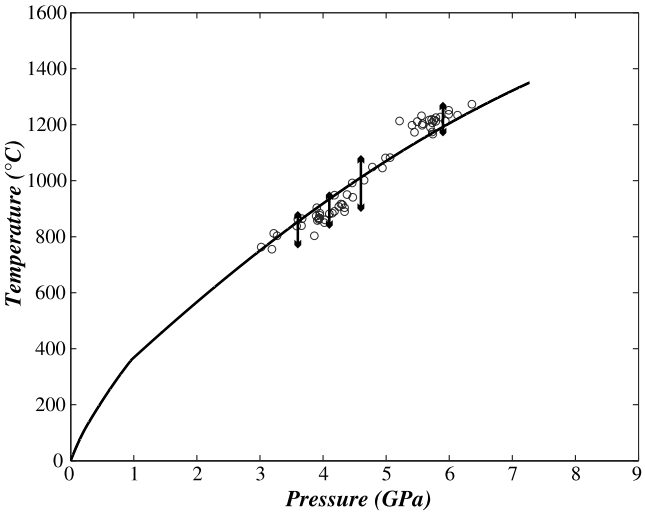

Figure 3. Xenolith (*P*,*T*) data from Kaapvaal orangeites (Newlands and Finsch), Kaapvaal craton, together with acceptable temperature ranges at several pressures. These temperature ranges account for uncertainties in both depth and temperature due to geobaromers and geothermometers. Additional constraints are that the surface heat flow must be between 40 and 46 mW m^{-2} and the basal temperature between 1250°C and 1550°C.

[25] The greatest uncertainty attends the deepest samples from the Finsch kimberlite. The subarray formed by the Finsch (*P*,*T*) data is not parallel to the geotherm defined by the entire data array. This difference could reflect real differences in the thermal structure of the lithosphere at this depth. However, it seems equally plausible that the entire Finsch xenolith suite was derived from a single pressure and temperature and that the observed scatter is due to a combination of analytical errors, minor compositional disequilibrium between minerals, and inaccurate compositional correction factors. The Finsch xenoliths derive from a depth range in which kimberlite-hosted xenoliths commonly show effect of metasomatic disturbance by the host magmatic event. In such case, the (*P*,*T*) array might not be geologically meaningful for the reasons mentioned above. We therefore decided not to assign too much weight to the slope defined by the Finsch array and averaged the Finsch data to provide only one more reliable but less restrictive constraint, defined by the whole data set at 5.9 GPa.

3.3. Additional Constraints

[26] In addition to xenolith (*P*,*T*) data, two other constraints are considered, involving surface heat flow, for which numerous measurements are available, and basal temperature.

[27] Heat flow in the Kaapvaal craton varies from 33 ± 2 mW m^{-2} in granitic domes to 51 ± 6 mW m^{-2} in the Witwatersrand basin [*Jones*, 1988]. This difference is apparently related to different crustal heat production values. In particular, the contribution to the surface heat flow in the basin from the 6-km-thick sequence of sedimentary rocks amounts to 7.5 mW m^{-2} [*Nicolaysen et al.*, 1981]. Subtracting this value from the surface heat flow leads to a subsediment heat flow of 43.5 mW m^{-2}. This value is in

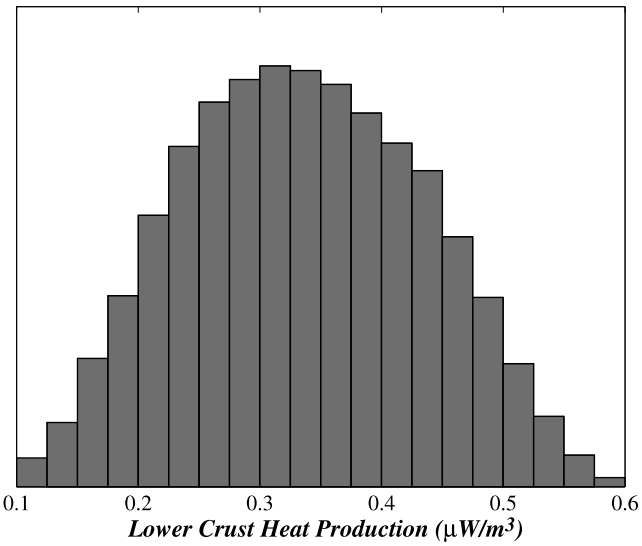

Figure 4. Distribution of values for heat production in the lower crust which are consistent with xenolith (*P*,*T*) data and constraints on surface heat flow values.

good agreement with measurements in the southern part of the craton, which show typical cratonic values of about 45 mW m^{-2} [*Jones*, 1992, 1998]. It is also very close to the average heat flow value for Archean cratons (41 ± 11 mW m^{-2} [*Nyblade et al.*, 1990]). Thus, surface heat flows of the selected models have to fall in the range 40 to 46 mW m^{-2}.

[28] At the base of the lithosphere, the temperature is taken to be between 1250 and 1550°C. The lower limit is estimated by examining the lowest temperature estimates from high-pressure xenolith data (Figure 3). This is the only basal boundary condition used in the present paper. Lithosphere thickness is an unknown which appears explicitly in the theoretical solutions and which is therefore solved for simultaneously with the other variables. In other words, lithosphere thickness is not determined as a consequence of the other parameter values and, in particular, is not defined by the intersection of the geotherm with an assumed isentropic profile. The range of basal temperatures for the Monte Carlo procedure is very large and does not depend on lithosphere thickness. Thus, the most powerful constraint on basal thermal conditions comes from the curvature of the temperature profile introduced by radioactive decay and secular transients.

4. First Set of Results for the Kaapvaal Craton

[29] Using xenolith (*P*,*T*) data and constraints on the surface heat flow and basal temperature we performed a first Monte Carlo inversion which gives preliminary results for the five main parameters of the model, A_{s0}, A_{m0}, H, Q_{b0}, and τ_s.

[30] The range of values allowed for heat production in the upper crust is tight because of the strong constraints that stem from heat flow data and direct measurements of U, Th, and K concentration in surface rocks. We find that all values within the range are equally probable, which shows that the range was determined properly. The distribution of values obtained for the lower crustal heat production is presented in Figure 4. The histogram shows a Gaussian-like probability density function centered on a rate of 0.34 μW m^{-3}, with a standard error of 0.08 μW m^{-3}. This value is in very good agreement with other estimates of lower crustal heat production from very different techniques, which argues for the consistency of this model. For instance, assuming that concentrations for a given rock type are valid throughout a geological province, *Pinet and Jaupart* [1987] calculated average values weighted by areal extent. For granulite-facies rocks, they found average heat production values tightly clustered around 0.4 μW m^{-3}, very close to the value we have obtained.

[31] Possible values for lithosphere thickness and present-day basal heat flow show important correlations with lithospheric mantle heat production. Probability densities for the couples (H,A_{m0}) and (Q_{b0},A_{m0}) are presented in Figure 5.

[32] Lithosphere thickness is well constrained between 190 and 270 km by (*P*,*T*) data and surface heat flow measurements, in comparison to the previously discussed

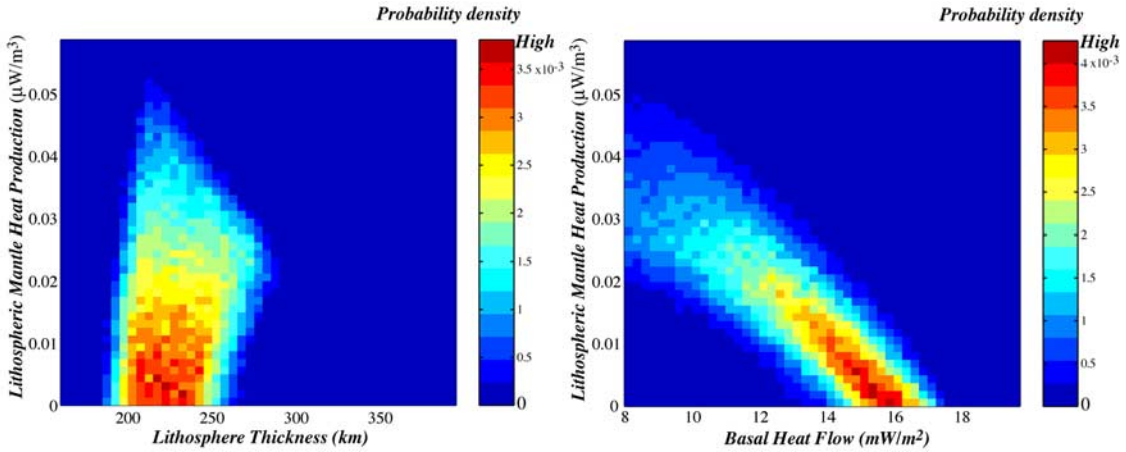

Figure 5. Probability density distributions for two sets of variables: present-day mantle heat production and lithosphere thickness (H,A_{m0}; left) and mantle heat production and basal heat flow (Q_{b0},A_{m0}; right) for successful models that satisfy xenolith (*P*,*T*) data as well as surface heat flow and basal temperature constraints for the Kaapvaal craton.

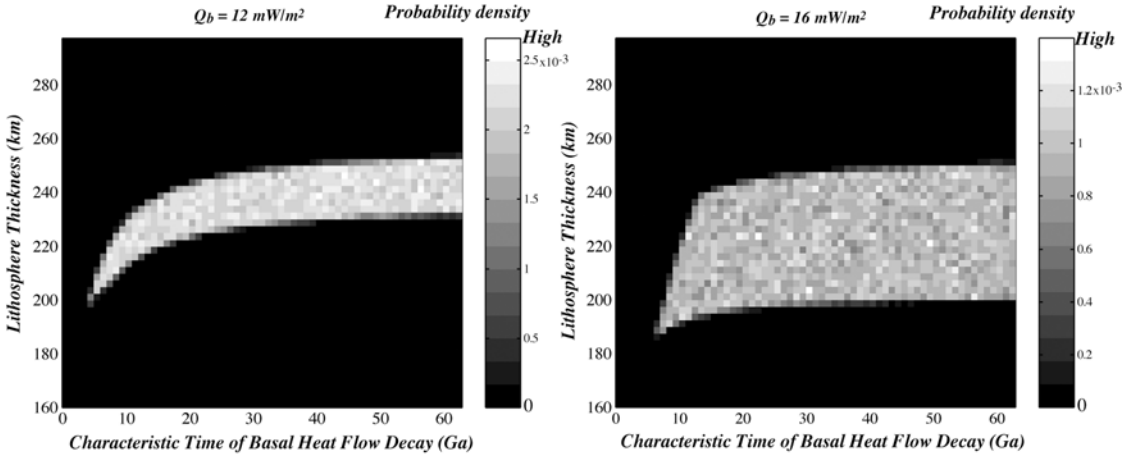

Figure 6. Probability density for the characteristic time of basal heat flow decay and lithosphere thickness (τ_s,H) in the Kaapvaal craton. For these calculations, values of heat production were set to the most probable values from the Monte Carlo inversion; A_{c0} = 1.55 μW m^{-3}, A_{s0} = 0.35 μW m^{-3}. Two extreme cases are shown: either a low basal heat flow, Q_{b0} = 12 mW m^{-2}, and a rate of heat generation in the mantle of 0.02 μW m^{-3} (left) or a high basal heat flow, Q_{b0} = 16 mW m^{-2}, and no heat produced in the mantle (right).

range of 160 to 400 km (Figure 5, left). The deeper lithosphere is obtained for a mantle heat production of about 0.025 μW m^{-3}. Concerning the probability density of lithosphere thickness alone, the mean value is 230 km, with a standard deviation of 18 km. Most probable values are thus between 210 and 250 km.

[33] Figure 5 shows that the most probable values for lithospheric mantle heat production are between 0 and 0.03 μW m^{-3}. The distribution of values for A_{m0} alone gives a mean of 0.017 μW m^{-3} within an interval extending from about 0.008 to 0.026μW m^{-3}. However, Figure 5 shows that the probability density for the couple (Q_{b0}, A_{m0}) is highest for lithospheric mantle heat production between 0 and 0.02 μW m^{-3}.

[34] Present-day basal heat flow is negatively correlated with mantle heat production. Most values are between 12 and 16 mW m^{-2} (Figure 5, right). Examining the distribution of basal heat flow alone gives a mean value of 12.7 mW m^{-2} with a range of 10.7–14.7 mW m^{-2}. This range differs a little from the correlated probability density because the higher the basal heat flow, the smaller the range for lithospheric mantle heat production is. This shows that it is important to consider the correlations between the different variables.

[35] The distribution of values for the characteristic time of basal heat flow decay, i.e., the characteristic time of secular cooling in the underlying mantle, is shown in Figure 6 as a function of lithosphere thickness for the two extreme cases of Figure 5. In one case, the basal heat flow is relatively low, 12 mW m^{-2}, and heat is produced in the lithospheric mantle at a rate of 0.02 μW m^{-3}. In the second case, the basal heat flow is relatively high, 16 mW m^{-2}, and no heat is generated in the mantle. No values less than 4 and 6 Ga are allowed for τ_s in the first and second cases respectively. The range of values for τ_s is smaller for the low basal heat flow value than for the larger one. For lithosphere thicker than 220 km, τ_s must be larger than 7.5 or 10 Ga in the first and second cases respectively. The deeper the continental root, the longer the thermal relaxation time. In such conditions, rapid variations of the basal heat flow would lead to marked curvature of the geotherm, which are not allowed by the xenolith data. Thus, τ_s increases with increasing lithosphere thickness. For very thick lithosphere, variations of basal heat flow must therefore be very small.

5. Comparison With the Slave Craton

5.1. Data and Constraints

[36] The present-day temperature profile of the Archean Slave craton, northwest Canada can also be well constrained using the thermobarometry of mantle-derived xenoliths within kimberlite pipes. Figure 7 shows Brey and Kölher

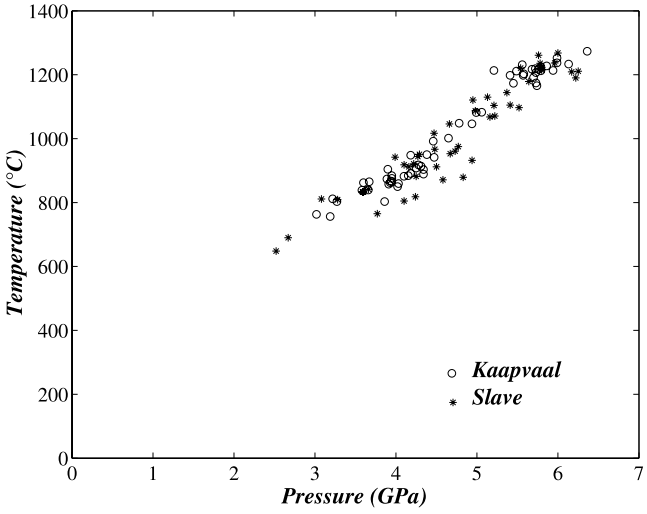

Figure 7. Pressure-Temperature data for mantle xenoliths coming from Jericho and Lac de Gras pipes, Slave craton, Canada (stars; *Russell and Kopylova* [1999] and (R. L. Rudnick, personal communication, 2003)), in comparison with data from Newlands and Finsch pipes, Kaapvaal craton, South Africa (circles).

Table 2. Parameters, Data and Constraints for the Slave Craton if Different From Those of the Kaapvaal Craton

Model Parameters	Symbol	A Priori Range of Values
Upper Crust Heat Production	A_{c0}	1.70–2.10 μW m^{-3}
Calculated Data	**Symbol**	**Acceptable Range of Values**
Temperature at 4.0 Gpa	$T_{4.0}$	810–950°C
Temperature at 4.5 Gpa	$T_{4.5}$	870–1000°C
Temperature at 5.0 Gpa	$T_{5.0}$	920–1130°C
Temperature at 5.5 Gpa	$T_{5.5}$	1080–1240°C
Temperature at 6.0 Gpa	$T_{6.0}$	1170–1270°C
First Set of Constraints	**Symbol**	**Acceptable Range of Values**
Surface Heat Flow	Q_s	44–52 mW m^{-2}
Temperature at $z = H, t = t_0$	T_b	1250–1550°C

thermobarometry data from different pipes in the Lac de Gras and Jericho area, north central part of the Slave craton, Canada [*Russell and Kopylova*, 1999], and how they compare to the data from the Newlands and Finsch pipes in the Kaapvaal craton. The Slave mantle lithosphere has usually been considered cooler than the Kaapvaal lithosphere because the main set of (P,T) estimates in the Kaapvaal, like Kimberley or Lesotho pipes, give substantially higher temperatures at depth than (P,T) estimates from the Slave craton. It is surprising how close the Newlands-Finsch and Jericho-Lac de Gras data are to one another. Another Monte Carlo procedure has thus been implemented, using Jericho and Lac de Gras xenolith (P,T) data from *Russell and Kopylova* [1999] and Rudnick (personal communication) as well as surface heat flow and heat production determinations in the same area of the Slave craton [*Mareschal et al.*, 2004]. We calculated the range of temperature at a given pressure following the same procedure as for the Kaapvaal craton. They are listed in Table 2.

[37] Few surface heat flow and heat production determinations are available in the Jericho-Lac de Gras area. *Mareschal et al.* [2004] measured temperature and heat production in two drill holes near Lac de Gras. They found a relatively high average surface heat flow of 46 ± 6 mW m^{-2} compared with other values for Archean province. This high surface heat flow is associated with a 10-km-thick enriched layer, characterized by a high heat production of about 1.9 μW m^{-3}. Other measurements in the area give a rate of heat generation of about 1.7 μW m^{-3} in the upper crust [*Thompson et al.*, 1995]. In the Yellowknife area, in the southern part of the craton, surface heat flow is higher, with a value of about 53 mW m^{-2}.

[38] For the Slave craton, we thus consider that the rate of heat generation in the upper crust is between 1.7 and 2.1 μW m^{-3}, higher than in the Kaapvaal craton. Surface heat flow has to fall in the range of 44–52 mW m^{-2}, and the basal temperature must be such that 1250°C < T_b < 1550°C, as before. Ranges of values for the other parameters have not been changed.

5.2. Lithosphere Thickness, Basal Heat Flow and Heat Production in the Slave Craton

[39] Results for the Jericho-Lac de Gras area, Slave craton, are similar to those for the Kaapvaal, as shown in Figure 8.

[40] The rate of heat generation in the lower crust has a mean value of 0.4 μW m^{-3}, with a standard deviation of 0.08 μW m^{-3}. These values are very close to those found for the Kaapvaal, suggesting that below an approximately 10-km-thick radioelement enriched layer, heat production is comparable to that in other Archean cratons.

[41] The mean lithosphere thickness is 235 km, a little higher than for the Kaapvaal, with a standard deviation of 18 km as well. It is well constrained between 200 and 280 km, and the deepest lithosphere is obtained for a mantle heat production of about 0.02 μW m^{-3} (Figure 8, left).

[42] We observed the same negative correlation between the present-day basal heat flow and mantle heat production (Figure 8, right). However, the solution domain is displaced toward lower values of basal heat flow and lithospheric mantle heat production with respect to the Kaapvaal. The mean heat production value is 0.016 μW m^{-3}, but, if we consider the probability density for the couple (A_{m0},Q_{b0}),

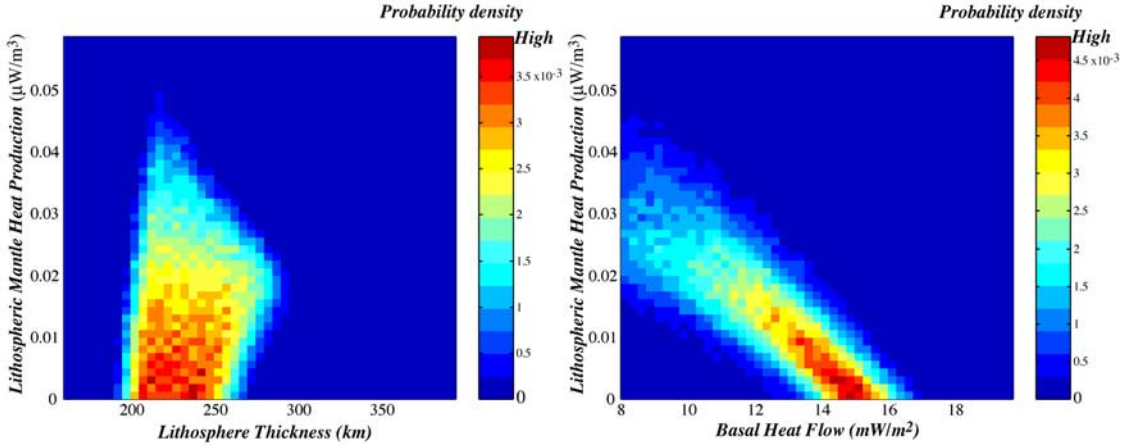

Figure 8. Probability density distributions for lithospheric parameters of the Slave province, Canada. Present-day mantle heat production and lithosphere thickness (H,A_{m0}; left) and present-day mantle heat production and basal heat flow (Q_{b0},A_{m0}; right). These are consistent with xenolith (P,T) data as well as with constraints on surface heat flow and on basal temperature for the Slave craton.

most probable values are somewhat smaller. This is also visible in Figure 8 (left), which shows the probability density for the couple (A_{m0},H).

[43] The mean of present-day basal heat flow values is 12 mW m^{-2}, with a standard deviation of 1.8 mW m^{-2}. The correlation between basal heat flow and mantle heat production shows, however, that most probable values are between 12 and 16 mW m^{-2}, close to the Kaapvaal results (Figure 8).

6. Tightening the Solution Space With Other Constraints

6.1. Additional Constraints

[44] So far, our analysis has led to parameter values that are consistent with the present-day thermal structure of the lithosphere as documented by xenolith data. The present-day geotherm, however, depends on radioactive decay and on the time variation of basal heat flow, which allows insights into the thermal evolution of the continental lithosphere and the underlying mantle. To obtain better models for thermal conditions in the past, we use additional time-dependent information. The Kaapvaal craton has been stable for about 3 Ga [*de Wit et al.*, 1992], implying that major melting has not occurred within the lithosphere since the Archean. Certain portions of the craton have been involved in large-scale melting events, giving rise to the Bushveld Complex, Ventersdorp, and Karoo eruptions, but the core of the craton appears unaffected, as shown by the presence of ancient (about 3 Ga) harzburgite-paragenesis diamonds [*Richardson et al.*, 1984; *Boyd et al.*, 1985] and abundant Archean Os isotope ages for peridotite xenoliths [*Pearson*, 1999]. Magmas from these events appear to have passed through the cratonic root in relatively narrow zones of long-term structural weakness [*Silver et al.*, 2004]. Another constraint can be drawn from geochemical estimates of cooling rates in the lithospheric mantle. Such estimates have been deduced from isotopic disequilibrium in xenolith minerals [*Bedini et al.*, 2004] and from comparative geothermobarometry of touching and non-touching inclusions within diamonds [*Girnis et al.*, 1999; *Phillips et al.*, 2004]. Both types of analysis lead to a range of about 40–110 K/Ga.

[45] The time-dependent model developed above permits calculation of the thermal structure of the continental lithosphere at any time and depth after the initial transient that follows root stabilization. For the purposes of this section, it is necessary to specify at what time this initial transient has run to completion. A numerical solution of the heat equation has therefore been carried out to follow the temporal evolution of the geotherm for different initial conditions. Results are presented in Appendices A and B for different models of thermal conductivity variations. Once the time-dependent model was validated by a full transient calculation, we introduced the other constraints in the Monte Carlo procedure. We further added a minimum thickness constraint and specifically required the rigid root to extend to at least 220 km. The thermal lithosphere, defined as the intersection between the conductive profile in the lithosphere and an assumed isentropic profile in the convecting mantle, is even deeper (Figure 1). A minimum depth of 220 km for the Kaapvaal craton is in good agreement with the most recent seismological studies [*James et al.*, 2001; *Gung et al.*, 2003].

[46] We have imposed the following conditions on the solutions:

[47] (1) A condition of no melting in the lithosphere since 2.5 Ga is equivalent to the requirement that the basal temperature was less than the solidus temperature 2.5 Ga ago. This condition is mathematically expressed as follows:

$$T(z = H, t = 2.5\ \text{Ga}) < T_{\text{solidus}} \tag{12}$$

where $T_{\text{solidus}} = 1800 + 70 \times (P(z = H) - 5.0)$ is in °C and P is in GPa, determined from the phase diagram of garnet lherzolite [*Herzberg*, 1983].

(2) Cooling rates determined from isotopic disequilibrium in mantle xenoliths from the Kaapvaal craton are in the range 40 to 110 K/Ga for pressures between 4.0 and 5.0 GPa [*Bedini et al.*, 2004]. This is written as follows:

$$40 < \overline{\left[\frac{\mathrm{d}T}{\mathrm{d}t}\right]}_{(P=4.0\ -\ 5.0\ \text{GPa},\ t=t_0)} < 110\ \text{K/Ga} \tag{13}$$

6.2. A Tighter Solution Space

[48] We performed two additional Monte Carlo inversions using this second set of constraints. In a first inversion, solutions are required to conform to the condition of no internal melting. In a second inversion, instantaneous cooling rates must correspond to the measured values.

[49] The distribution of heat production values in the crust changes little from the results obtained with the first set of constraints and is not discussed further.

[50] The probability density for the couple Q_{b0}, A_{m0}, (basal heat flow – mantle heat production) is shown in Figure 9 for the two new conditions. The field of possible values is significantly reduced in comparison to the first set of results (Figure 5, right). For the condition of no melting, no solution exists for heat production values greater than 0.04 μW m^{-3} and basal heat flow less than 9 mW m^{-2}. The cooling rate condition restricts the results even further, with an upper bound of 0.03 μW m^{-3} for heat production and a lower bound of 11 mW m^{-2} for the basal heat flow. Both conditions, however, lead to almost the same total range for these variables: 0–0.02 μW m^{-3} for lithospheric mantle heat production and 12–16 mW m^{-2} for the present-day basal heat flow.

[51] The solutions that have been selected in this manner correspond to a relatively deep lithosphere (H > 220 km) and imply rather small rates of secular cooling. Heat production in the lithospheric mantle is pushed toward low values, which causes the distribution of basal heat flow values to be skewed toward high values. All else being equal, the higher the present-day basal heat flow, the higher the secular cooling rate. Thus, because xenolith data are not consistent with large curvature in the geotherm, the characteristic time for basal heat flow decay is higher than for the first set of constraints.

[52] Thermal transients due to radioactive decay within the lithosphere and to secular decrease of the basal heat flow are best discussed in terms of temperature changes at the

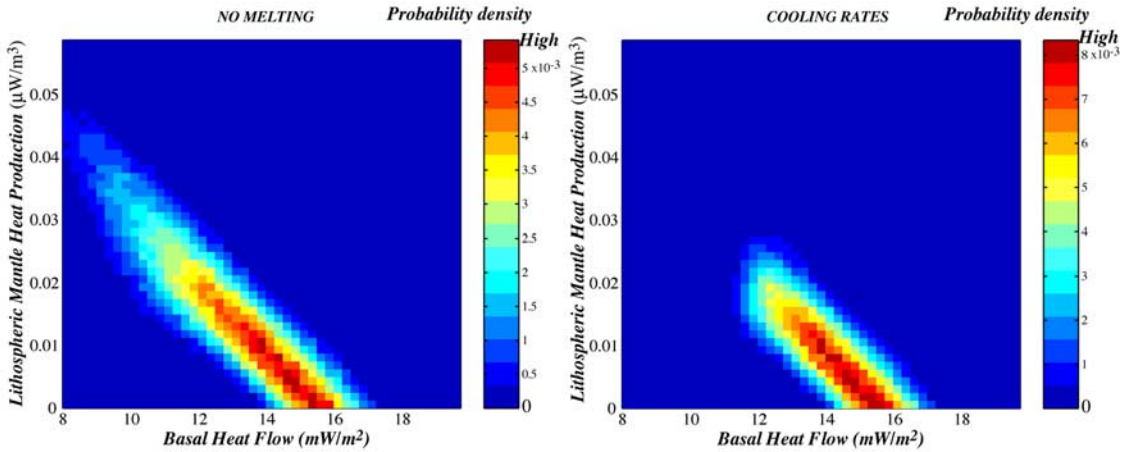

Figure 9. Probability density for present-day radioactive heat production values in the lithospheric mantle and basal heat flow (Q_{b0},A_{m0}) for successful models which satisfy constraints on basal temperature and surface heat flow and a minimum lithosphere thickness $H > 220$ km. Additional constraints are a condition of no melting within the lithosphere over 2.5 Ga (left) and cooling rates derived from geochemical studies (right).

base of the lithosphere, i.e., cooling in the lithosphere and in the underlying mantle.

7. Discussion

7.1. Heat Production in the Lithosphere

[53] In thick lithosphere, even small amounts of radioelements may have a large impact on thermal structure and surface heat flow. Consider for example that the heat generation rate is 0.03 μW m^{-3} in a 235-km-thick lithospheric mantle (corresponding to a total thickness of 270 km), the heat flow component due to radioactive decay in the lithospheric mantle is 7 mW m^{-2}. This is almost as large as the basal heat flow and more than one-fourth of the amount of heat generated in the crust. Thus, thermal models of continental lithosphere can only be accurate if they rely on exact values of heat production in the lithospheric mantle.

[54] The Monte Carlo procedure leads to values of crustal heat production that are higher in the Slave than in the Kaapvaal: mean values are 0.76 and 0.70 μW m^{-3} respectively. This is consistent with the enriched nature of the Slave upper crust. Below the upper crust, heat production takes similar values in the Slave and the Kaapvaal, both in the lower crust and in the lithospheric mantle. Upon closer scrutiny, the lithospheric mantle may be slightly more depleted in the Slave than in the Kaapvaal. For instance, if we consider that the basal heat flow is the same beneath both provinces, heat production in the Slave lithospheric mantle is smaller than in the Kaapvaal by about 0.007 μW m^{-3}. This difference may come from metasomatic processes which seem to have been very active in the Kaapvaal cratonic root. Alternatively, the difference may be due to crust extraction from the mantle. If the Slave and Kaapvaal crusts have been extracted from the underlying roots, the Slave root should be more depleted than the Kaapvaal one. For example, the difference of bulk crustal heat production between the two cratons corresponds to a difference of about 0.01 μW m^{-3} in 210-km-thick lithospheric mantle, which is consistent with our results.

7.2. Lithosphere Thickness

[55] The thickness of the conductive boundary layer is between 200 and 270 km, with preferred values between 210 and 250 km. Very consistent values have been obtained for the Kaapvaal and Slave cratons. The whole thermal boundary layer, which includes the rigid lid and the convective boundary layer below, is thicker (Figure 1). *Jaupart et al.* [1998] estimated a thickness of a few tens of kilometers for the convective boundary layer using a parameterization for the convective heat flux. Thus, the whole thermal boundary layer extends to a depth of at least 230 km and possibly to as much as 300 km beneath the Kaapvaal.

[56] These thickness values are consistent with seismological estimates, but exceed most estimates from petrology. The thermally determined thickness is an average over a horizontal distance of at least 300 km [*Mareschal and Jaupart*, 2004], whereas seismic tomography suggests that the thickness of the Kaapvaal root varies laterally [*James et al.*, 2001]. Seismic velocities, however, depend on composition as well as on temperature so that some of the apparent thickness variations could be due to compositional differences. Petrologic studies also suggest lateral variations within the craton interior [*Griffin et al.*, 2003; *Bell and Moore*, 2004]. These are inferred to have a strong temporal component [*Bell et al.*, 2003; *Griffin et al.*, 2003]. *Griffin et al.* [2003] proposed a change in average lithospheric thickness from about 210 to 180 km just before the second and main kimberlite phase about 100 Ma ago. Indeed, a significant fraction of the seismically inferred lateral variations could derive from magmatic and metasomatic effects associated with, and following breakup of, the Gondwana supercontinent at ≈200 Ma.

[57] The apparent discrepancy between the petrologic and other estimates of lithospheric thickness may derive in part

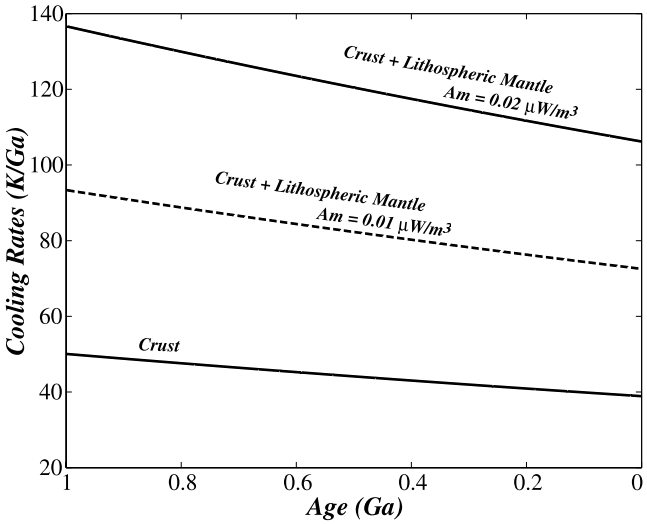

Figure 10. Cooling rates as a function of age due to in situ radioactive decay in the lithosphere, calculated at the base of the lithosphere. Parameters are as follows: $H = 240$ km, $A_{c0} = 1.55$ μW m^{-3}, and $A_{s0} = 0.35$ μW m^{-3}. Results for two different rates of heat production in the lithospheric mantle are shown ($A_{m0} = 0$, 0.01, and 0.02 μW m^{-3}). These results meet all constraints available, including the no-melting condition.

from influences of the xenolith sampling process in the mantle. Thickness of the petrologically determined lithosphere is defined by the transition from melt-depleted to melt-metasomatized compositions. It is possible that metasomatism is enhanced in the neighborhood of kimberlite pipes, i.e., that kimberlites erupt in areas where metasomatism has infiltrated the lithosphere to shallow levels. Samples from these regions might therefore yield thinner estimates than those estimates derived remotely from the geophysical properties of the ambient cratonic mantle.

7.3. Cooling in the Lithosphere

[58] We have obtained constraints on heat production rates in the lithospheric mantle and in the crust and hence can calculate the cooling rates that are implied for the lithosphere using equation (8). Figure 10 presents cooling rates at the base of 240-km-thick lithosphere as a function of age for mean values of heat production in the crust and for two different values of heat production in the mantle. Crustal heat sources alone are responsible for a cooling rate of about 40 K/Ga. Adding heat sources in the lithospheric mantle, the total cooling rate due to in situ radioactive decay may be as large as 110 K/Ga at the base of the lithosphere.

[59] Heat production may be zero in the lithospheric mantle, in which case the only decaying heat sources are those of the crust. We thus arrive at a range of about 40–110 K/Ga for the radioactivity-induced cooling rate. This accounts for a large fraction of the cooling rate determined from isotopic disequilibria in lithospheric minerals [*Bedini et al.*, 2004]. This estimate also compares favorably with the maximum of ≈50 K/Ga deduced from diamond inclusion thermometry between 4.5 and 6.5 GPa [*Phillips et al.*, 2004]. This indicates that only a small amount of lithospheric cooling can be attributed to secular changes of heat supply from the convective mantle.

[60] We have calculated the amount of cooling due to changes of basal heat flow. At the base of the lithosphere, this corresponds to the secular temperature change of the convective mantle below the root. Figure 11 shows these calculated cooling rates as a function of the rate of heat generation in the lithospheric mantle. The larger the rate of heat generation, the larger the radioactivity-induced cooling, and hence the smaller the amount of cooling due to basal heat flow decrease. For both sets of constraints, there are no solutions larger than 80 K/Ga and the probability increases toward the lowest values. Most values are less than 40 K/Ga. These results provide the first direct estimates of secular cooling in the underlying mantle, i.e., based on (P,T) data. They are much smaller than estimates from so-called parameterized cooling models for the Earth [*Schubert et al.*, 1980],

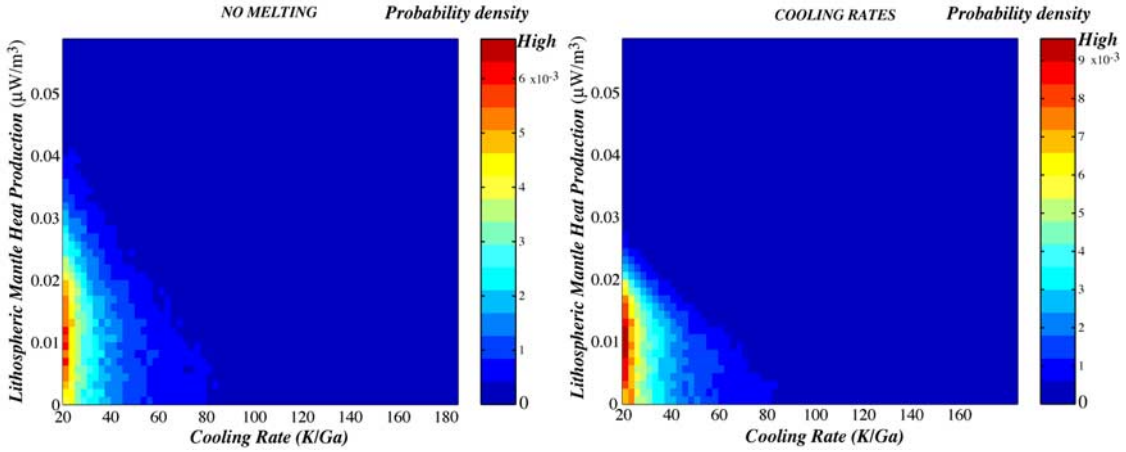

Figure 11. Probability density of the cooling rates in mantle below the lithosphere due to secular changes of basal heat flow (in K/Ga) as a function of lithospheric mantle heat production for two types of constraints: left, condition of no melting; right, values of the cooling rate deduced from geochemical studies. These two constraints lead to similar results. The cooling rate constraint is more restrictive. Most values are less than 40 K/Ga.

using Urey ratio of ≈0.7. They suggest that the mantle beneath the continental lithosphere cools more slowly than the entire mantle or that parameterized models estimate cooling rates that are too large. Local cooling rates below continents need not be representative of global cooling rates. *Lenardic et al.* [2005] and *Lenardic* [2006] have suggested that continental insulation acts to increase the average mantle temperature, thereby increasing heat flux through ocean basins and enhancing the difference between oceanic and continental heat fluxes. Other parameterized models that consider a weaker dependence of the heat flow on the mantle temperature, as suggested by *Christensen* [1985], or that take into account the effect of more sluggish plate tectonics in the past because of stiffer more depleted plates [*Korenaga*, 2006] predict cooling rates that are smaller than the parameterized models. These models, however, predict a cooling of at least 150 K for the last 3 Ga, i.e., in the upper range of our results.

8. Conclusion

[61] We have presented a set of continental geotherms that are intrinsically time-dependent because of in situ radioactive decay and have compared them to (*P*,*T*) data derived from mineral compositions in xenoliths from the lithospheric roots of the Kaapvaal, South Africa and Slave, Canada. In both cratons, heat production in the lower crust is estimated to be about 0.3 to 0.4 μW m^{-3}. Lithosphere thickness, defined as the purely conductive part of the lithosphere, is constrained to lie within a range of 210–250 km, which implies that the thermal boundary layer of Archean continents extends to a depth of at least 230 km. Requiring that past temperatures in continental roots never reached the solidus and decayed at rates that are consistent with geochemical constraints, we have obtained an upper bound of 0.03 μW m^{-3} for the rate of radiogenic heat production in the lithospheric mantle. Heat flow at the base of the rigid lithosphere must lie within a range of 12–16 mW m^{-2}, less than what is usually assumed for the Kaapvaal. This method provides the first estimate of the rate of secular cooling in the mantle relying on xenolith (*P*,*T*) data. Cooling rates thus estimated are less than 40 K/Ga, much less than typical parameterized cooling models and still less than more sophisticated models accounting for rigid plate tectonics. One explanation may be that such cooling rates are local values below cratons which do not hold for the entire mantle. Another explanation may be that theoretical cooling models are not accurate.

Appendix A: Temperature-Dependent Thermal Conductivity

[62] Solutions of the heat equation with temperature-dependent conductivity have been obtained numerically.

[63] Measurements of conductivity or diffusivity values in olivine under upper mantle conditions show that it depends on pressure and temperature [*Katsura*, 1995]. For the depth range of interest here, however, the effect of pressure can be neglected. With this assumption, the heat equation becomes:

$$\rho C_P \frac{\partial T}{\partial t} = \frac{\partial}{\partial z}\left(k(T)\frac{\partial T}{\partial z}\right) + A_i(t) \qquad \text{(A1)}$$

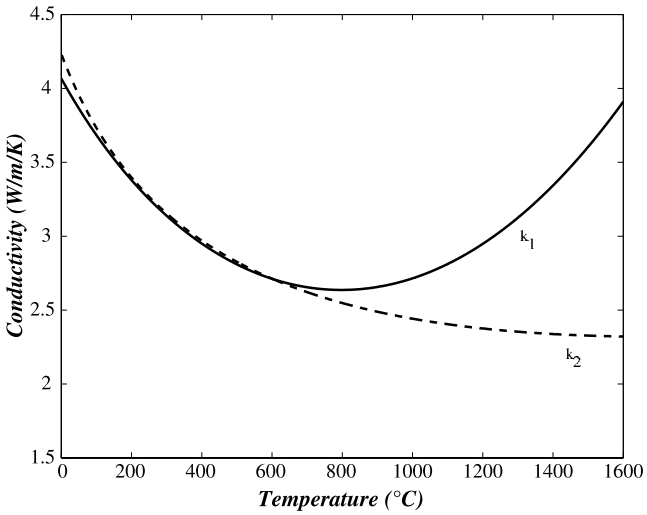

Figure A1. Two different models for the thermal conductivity k as a function of temperature in the lithospheric mantle, k_1 shows a positive temperature dependence at higher temperature, contrary to model k_2, because of the importance of radiative heat transfer at high temperature.

with $i = c$, s, and m for the upper crust, lower crust, and mantle heat production respectively. We have obtained solutions for the transient evolution of a 220-km-thick lithosphere starting 3.5 Ga ago. The initial thermal structure is such that the lower crust is close to melting, at a temperature of 800°C, and the base of the lithosphere is at 1450°C. Other initial conditions have been used with no difference in the final result because thermal relaxation of the initial thermal structure occurs in about 1 Ga.

[64] In the crust, conductivity is kept constant with a typical average value of 2.55 W m^{-1} K^{-1}. We have considered two different models for the variation of the mantle thermal conductivity with temperature in order to evaluate the associated uncertainties. In a first case, we rely on the laboratory data of *Schatz and Simmons* [1972], *Schärmeli* [1979], *Roy et al.* [1981], and *Katsura* [1995], such that the effect of radiative heat transport becomes important at about 800°C (Figure A1):

$$k_1(T) = \frac{1}{0.174 + 0.000265T} + 0.368 \times 10^{-9} T^3 \qquad \text{(A2)}$$

where T is in Kelvin. For this equation, the average conductivity value in the range 273–1600 K is 3.0 W m^{-1} K^{-1}. *Katsura* [1995] proposed an almost constant thermal diffusivity value of 0.7–0.8 $\times$ 10^{-6} m^2 s^{-1} for the upper mantle.

[65] *Xu et al.* [2004] have recently proposed the following equation for lattice conduction in olivine at 4.0 GPa:

$$k_1(T) = k_0\left(\frac{298}{T}\right)^n \qquad \text{(A3)}$$

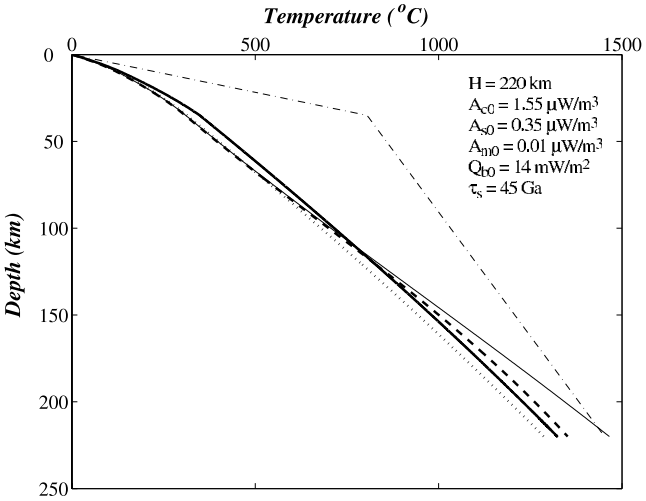

Figure A2. Present-day vertical temperature profiles for a 220-km-thick lithosphere for three different models of thermal conductivity variations with temperature. Dashed-dotted line: initial temperature profile 3.5 Ga ago. Thick dashed line: temperature-dependent thermal conductivity $k_1(T)$. Thin solid line: temperature-dependent conductivity $k_2(T)$. Dotted line: constant conductivity, $k = 3.0$ W m^{-1} K^{-1} in the mantle. The analytical solution is shown for comparison in the thick solid line for a constant conductivity of 3.0 W m^{-1} K^{-1} in the mantle.

where T is in Kelvin, $k_0 = 4.08$, $n = 0.406$. As for the radiative contribution, *Hofmeister* [1999] gave a simple polynomial expression:

$$k_r(T) = \sum_{m=0}^{3} d_m T^m \tag{A4}$$

where T is in Kelvin, and the values for the constant are $d_0 = 1.753 \times 10^{-2}$, $d_1 = -1.0365 \times 10^{-4}$, $d_2 = 2.2451 \times 10^{-7}$, and $d_3 = 3.4071 \times 10^{-11}$. In a second case, we consider the sum of both of these contributions:

$$k_2(T) = k_1(T) + k_r(T) \tag{A5}$$

Radiative heat transfer is much less important in this case than in the previous one, and conductivity decreases in a monotonic fashion with increasing temperature (Figure A1).

[66] We have solved equation (A1) with the same boundary conditions as in the model with constant properties: temperature is kept equal to zero at the surface, and both the basal heat flow and the rate of radiogenic heat production decrease exponentially with time. The integration is calculated using a fourth-order Runge-Kutta scheme.

[67] In a third calculation, we have taken a constant conductivity for the lithospheric mantle equal to 3 W m^{-1} K^{-1} for comparative purposes. This also allows an evaluation of the initial thermal relaxation phase.

[68] Figure A2 gives present-day temperature profiles for the three conductivity models, for a 220-km-thick conductive lithosphere starting 3.5 Ga ago. For all cases, heat productions are 1.55 μW m^{-3} in the upper crust, 0.35 μW m^{-3} in the lower crust, and 0.02 μW m^{-3} in the lithospheric mantle. The present-day value of the basal heat flow is 14 mW m^{-2} with a characteristic decay time of 45 Ga. We also show the present-day analytical solution for the secular thermal evolution with the same parameter values and a constant thermal conductivity of 3.0 W m^{-1} K^{-1} in the lithospheric mantle.

[69] Today, after 3 Ga of evolution, the temperature profile calculated with a constant mantle thermal conductivity is very close to the analytical solution. At all depths, the difference between the two is less than 40 K, which may be considered negligible compared with errors on xenolith (P,T) data. This calculation validates our transient model and also shows that the initial thermal profile has no influence on the present-day final shape of the geotherm and that thermal relaxation has proceeded to completion.

[70] For model 1, which gives an average conductivity value of 3.0 W m^{-1} K^{-1} in the range 273–1600 K, the resulting temperature profile is also very close to the analytical solution with a constant thermal conductivity value: the difference between the two is less than 30 K. The second conductivity function $k_2(T)$ is for all practical purposes identical to $k_1(T)$ up to a temperature of about 800°C. At this point, the difference between the two functions increases and this leads to significant differences in the calculated temperature profiles at depths larger than 120 km. This is due to the smaller values of conductivity at those depths, which act to slow down heat transport. The difference between the two profiles is largest at the base of the lithosphere, at a depth of 220 km, where it reaches 150 K. The agreement between the profiles calculated for conductivity function k_1 and a constant conductivity shows that the analytical solution is sufficiently accurate provided that the conductivity models have the same average value over the temperature range of interest. For a good fit to the second conductivity function, a smaller value of the average conductivity should be used in the analytical solution. Using the $k_2(T)$ conductivity function would have easily predict-

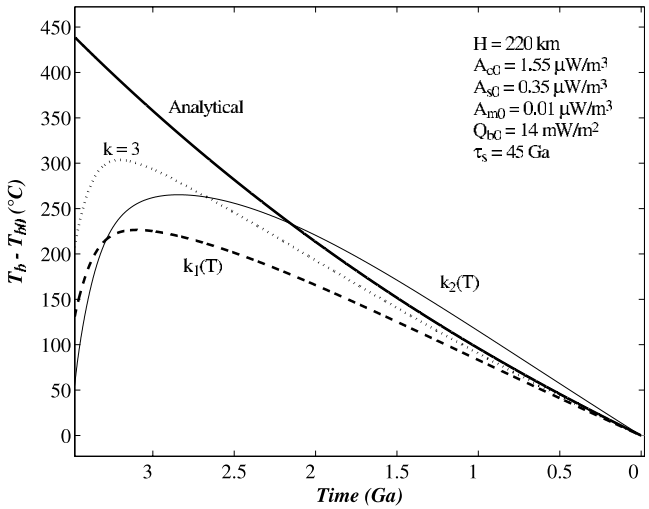

Figure B1. Cooling at the base of the lithosphere, i.e., difference between the basal temperature at time t and the present-day one for three different models for thermal conductivity variations. Calculations are as in Figure A2. Results for the present-day mantle are almost identical.

able consequences for a given lithosphere thickness, values of heat production in the lithospheric mantle would be larger and changes of basal heat flow would be less than for the $k_1(T)$ conductivity function. We prefer to use the latter function because it relies on a larger number of independent laboratory measurements.

Appendix B: Testing the Time Dependence of the Model

[71] Using three different models of conductivity, $k_1(T)$, $k_2(T)$ and a constant conductivity $k_3 = 3.0$ W m^{-1} K^{-1}, we have calculated numerically the evolution of temperature at the base of the continental lithosphere (Figure B1). In all cases, the secular cooling trend is attained quickly, after about 500 Ma. For times larger than this, thermal evolution is dominated by the rundown of radioelements and the basal heat flow decrease.

Appendix C: Analytical Solutions for the Instantaneous Geotherm With Four Heating Components

[72] For $0 \le z \le s$

$$Z_c(z) = \frac{A_{c0}\tau_r}{\rho C_P}[a_{c1}\cos(r_1 z) + b_{c1}\sin(r_1 z) - 1]$$

$$Z_s(z) = \frac{A_{s0}\tau_r}{\rho C_P}[a_{s1}\cos(r_1 z) + b_{s1}\sin(r_1 z)]$$

$$Z_m(z) = \frac{A_{m0}\tau_r}{\rho C_P}[a_{m1}\cos(r_1 z) + b_{m1}\sin(r_1 z)]$$

$$Z_b(z) = x_1\cos(r_2 z) + y_1\sin(r_2 z)$$

[73] For $s \le z \le d$

$$Z_c(z) = \frac{A_{c0}\tau_r}{\rho C_P}[a_{c2}\cos(r_1(z-s)) + b_{c2}\sin(r_1(z-s))]$$

$$Z_s(z) = \frac{A_{s0}\tau_r}{\rho C_P}[a_{s2}\cos(r_1(z-s)) + b_{s2}\sin(r_1(z-s)) - 1]$$

$$Z_m(z) = \frac{A_{m0}\tau_r}{\rho C_P}[a_{m1}\cos(r_1 z) + b_{m1}\sin(r_1 z)]$$

$$Z_b(z) = x_1\cos(r_2 z) + y_1\sin(r_2 z)$$

[74] For $d \le z \le H$

$$Z_c(z) = \frac{A_{c0}\tau_r}{\rho C_P}[a_{c3}\cos(r_1(z-d)) + b_{c3}\sin(r_1(z-d))]$$

$$Z_s(z) = \frac{A_{s0}\tau_r}{\rho C_P}[a_{s3}\cos(r_1(z-d)) + b_{s3}\sin(r_1(z-d))]$$

$$Z_m(z) = \frac{A_{m0}\tau_r}{\rho C_P}[a_{m2}\cos(r_1(z-d)) + b_{m2}\sin(r_1(z-d)) - 1]$$

$$Z_b(z) = x_2\cos(r_2(z-d)) + y_2\sin(r_2(z-d))$$

with $r_1 = \sqrt{\frac{1}{\kappa\tau_r}}$ and $r_2 = \sqrt{\frac{1}{\kappa\tau_s}}$

$$a_{c1} = 1$$

$$b_{c1} = [k_c \times (\sin(r_1 d) - \sin(r_1(d-s))) + 2k_m \sin\left(r_1\frac{s}{2}\right) \times \sin\left(r_1\left(d-\frac{s}{2}\right)\right)\tan(r_1(d-H))]\Big/ D_1$$

$$a_{s1} = 0$$

$$b_{s1} = \left[k_c \sin(r_1(d-s)) + 2k_m \tan(r_1(d-H))\left(\sin\left(r_1\frac{d-s}{2}\right)\right)^2\right]\Big/ D_1$$

$$a_{m1} = 0$$

$$b_{m1} = \frac{k_m}{k_c}\tan(r_1(H-d)) \times \left[\cos(r_1 d)\left(1 - \frac{k_m}{k_c}\tan(r_1(H-d))\tan(r_1 d)\right)\right]^{-1}$$

$$a_{c2} = \left(\sin\left(r_1\frac{s}{2}\right)\right)^2[(k_c + k_m)\cos(r_1(H-s)) + (k_c - k_m)\cos(r_1(H-2d+s))] \times [D_1\cos(r_1(H-d))]^{-1}$$

$$b_{c2} = \left(\sin\left(r_1\frac{s}{2}\right)\right)^2[(k_c + k_m)\sin(r_1(H-s)) + (k_m - k_c)\sin(r_1(H-2d+s))] \times [D_1\cos(r_1(H-d))]^{-1}$$

$$a_{s2} = k_m\sin(r_1 s)\tan(r_1(d-H))/D_1 + \cos(r_1 s) \times (k_c\cos(r_1(d-s)) - k_m\sin(r_1(d-s))\tan(r_1(H-d)))/D_1$$

$$b_{s2} = \cos(r_1 s) \times \left[k_c\sin(r_1(d-s)) + 2k_m\tan(r_1(d-H))\left(\sin\left(r_1\frac{d-s}{2}\right)\right)^2\right]\Big/ D_1$$

$$a_{c3} = 4k_c\cos(r_1(H-d)) \times \left(\sin\left(r_1\frac{s}{2}\right)\right)^2\Big/ D_2$$

$$b_{c3} = 2k_c\tan(r_1(H-d)) \times \left(\sin\left(r_1\frac{s}{2}\right)\right)^2\Big/ D_1$$

$$a_{s3} = k_c(\cos(r_1 s) - \cos(r_1 d))$$

$$b_{s3} = 2k_c \tan(r_1(H-d)) \sin\left(r_1 \frac{d-s}{2}\right) \sin\left(r_1 \frac{d+s}{2}\right) \Big/ D_1$$

$$a_{m2} = \left[1 - \frac{k_m}{k_c} \tan(r_1(H-d)) \tan(r_1 d)\right]^{-1}$$

$$b_{m2} = \tan(r_1(H-d)) \times \left[1 - \frac{k_m}{k_c} \tan(r_1(H-d)) \tan(r_1 d)\right]^{-1}$$

$$x_1 = 0$$

$$y_1 = Q_{b0} \times [r_2 \cos(r_2(H-d))D_3]^{-1}$$

$$x_2 = Q_{b0} \sin(r_2 d) \times [r_2 \cos(r_2(H-d))D_3]^{-1}$$

$$y_2 = \frac{k_c}{k_m} Q_{b0} \cos(r_2 d) \times [r_2 \cos(r_2(H-d))D_3]^{-1}$$

$$D_1 = k_c \cos(r_1 d) + k_m \sin(r_1 d) \tan(r_1(H-d))$$

$$D_2 = (k_c + k_m) \cos(r_1 d) + (k_c - k_m) cos(r_1(H-2d))$$

$$D_3 = k_c \cos(r_2 d) - k_m \sin(r_2 d) \tan(r_2(H-d))$$

Appendix D: Two Thermal Components in the Lithospheric Mantle

[75] Phlogopite, a potassium-rich mineral, is the main repository of radioactive elements in the lithospheric mantle. It is a stable phase down to a depth of about 180 km and to a temperature of about 1200°C [*Sudo and Tatsumi*, 1990]. Thus, one may expect that the upper part of the lithospheric mantle is enriched in radioactive elements compared with the lower part of it. The effect of enhanced heat production in the ''upper lithospheric mantle'' would be to increase the curvature of the temperature profile near the transition depth of about 180 km. We have therefore determined the analytical solution for five heating components, the upper and lower crust, the upper and lower lithospheric mantle, and the basal heat flow. We carried out a Monte Carlo inversion with one additional heating parameter (i.e., allowing for separate values of heat production in the ''upper'' and ''lower'' lithospheric mantle). We found no significant difference with the results for a homogeneous lithospheric mantle because few xenolith (*P*,*T*) data are available at depths larger than 180 km (Figure 7). Indeed, we considered only one constraint for the deepest parts of the lithosphere, at a pressure of 5.9 GPa.

[76] **Acknowledgments.** We thank Adrian Lenardic and Graham Pearson for their comments and suggestions. This work was funded by the Agence Nationale de la Recherche, France.

References

Bedini, R. M., J. Blichert-Toft, M. Boyet, and F. Albarède (2004), Isotopic constraints on the cooling of the continental lithosphere, *Earth Planet. Sci. Lett.*, *223*, 99–111.

Bell, R. (2002), Internally consistent geothermobarometers for garnet harzburgites: Model refinement and application, *Eos Trans. AGU*, *83*(47), Fall Meet. Suppl., Abstract T61A-1243.

Bell, D. R., and R. O. Moore (2004), Deep chemical structure of the southern African mantle from kimberlite megacrysts, *S. Afr. J. Geol.*, *107*, 59–80.

Bell, D. R., M. D. Schmitz, and P. E. Janney (2003), Mesozoic thermal evolution of the southern African mantle lithosphere, *Lithos*, *71*, 273–287.

Boyd, F. R., and J. J. Gurney (1986), Diamonds in the African lithosphere, *Science*, *232*, 472–477.

Boyd, F. R., and R. H. McCallister (1976), Densities of fertile and sterile garnet lherzolites, *Geophys. Res. Lett.*, *3*, 509–512.

Boyd, F. R., J. J. Gurney, and S. H. Richardson (1985), Evidence for a 150–200 km thick Archean lithosphere from diamond inclusion thermobarometry, *Nature*, *315*, 387–389.

Brey, G. P., and T. Kohler (1990), Geothermobarometry in four-phase lherzolites. II. New thermobarometers, and practical assessment of existing thermobarometers, *J. Petrol.*, *31*, 156–180.

Canil, D., and H. S. O'Neill (1996), Distribution of ferric iron in some upper mantle assemblages, *J. Petrol.*, *37*, 609–635.

Carswell, D. A. (1991), The garnet-orthopyroxene Al barometer: Problematic application to natural garnet lherzolite assemblages, *Mineral. Mag.*, *55*, 19–31.

Christensen, U. (1985), Thermal evolution models for the Earth, *J. Geophys. Res.*, *90*, 2995–3007.

de Wit, M. J., C. Roering, R. J. Hart, R. A. Armstrong, C. E. J. de Ronde, R. W. E. Green, M. Tredoux, E. Peberdy, and R. A. Hart (1992), Formation of an Archean continent, *Nature*, *357*, 553–562.

Girnis, A. V., T. Stachel, G. P. Brey, J. W. Harris, and D. Phillips (1999), Internally consistent geothermobarometers for garnet harzburgites: Model refinement and application, in *Proceedings of the 7th International Kimberlite Conference, Cape Town*, The J.B Dawson Volume. Red Roof Design, Cape Town, pp. 247–254.

Grégoire, M., D. R. Bell, and A. P. Le Roex (2003), Garnet lherzolites from the Kaapvaal craton (South Africa): Trace element evidence for a metasomatic history, *J. Petrol.*, *44*, 629–657.

Griffin, W. L., S. Y. O'Reilly, L. M. Natapov, and C. G. Ryan (2003), The evolution of lithospheric mantle beneath the Kalahari craton and its margin, *Lithos*, *71*, 215–241.

Guillou, L., and C. Jaupart (1995), On the effects of continents on mantle convection, *J. Geophys. Res.*, *100*, 24,217–24,238.

Gung, Y., M. Panning, and B. Romanowicz (2003), Global anisotropy and the thickness of continents, *Nature*, *422*, 707–711.

Gurney, J. J., and B. Harte (1980), Chemical variations in upper mantle nodules from southern African kimberlites, *Philos. Trans. R. Soc.*, 273–293.

Herzberg, C. T. (1983), Solidus and liquidus temperatures and mineralogies for anhydrous garnet lherzolite to 15 GPa, *Phys. Earth Planet. Inter.*, *32*, 193–202.

Hofmeister, A. (1999), Mantle values of thermal conductivity and geotherm from phonon lifetimes, *Science*, *283*, 1699–1709.

Hops, J. J., J. J. Gurney, B. Harte, and P. Winterburn (1989), Megacrysts and high temperature nodule from the Jagersfontein kimberlite pipe, in *Kimberlites and Related Rocks. Volume 2. Their Mantle/Crust Setting, Diamonds and Diamond Exploration*, vol. 14, pp. 759–770, Geological Society Australia Spec. Publ.

James, D. E., M. J. Fouch, J. C. VanDecar, and S. Van der Lee (2001), Tectospheric structure beneath southern Africa, *Geophys. Res. Lett.*, *28*(13), 2485–2488.

Jaupart, C., and J. C. Mareschal (1999), The thermal structure and thickness of continental roots, *Lithos*, *48*, 93–114.

Jaupart, C., J. C. Mareschal, L. Guillou-Frottier, and A. Davaille (1998), Heat flow and thickness of the lithosphere in the Canadian shield, *J. Geophys. Res.*, *103*, 15,269–15,286.

Jones, M. Q. W. (1988), Heat flow in the Witwatersrand basin and environs and its significance for the South African shield geotherm and lithosphere thickness, *J. Geophys. Res.*, *93*, 3243–3260.

Jones, M. Q. W. (1992), Heat flow anomaly in Lesotho: Implications for the southern boundary of the Kaapvaal craton, *Geophys. Res. Lett.*, *19*, 2031–2034.

Jones, M. Q. W. (1998), A review of heat flow in southern Africa and the thermal structure of the lithosphere, *South. Afr. Geophys. Rev*, *2*, 115–122.

Jordan, T. H. (1975), The continental tectosphere, *Rev. Geophys. Space Phys.*, *13*, 1–12.

Jordan, T. H. (1988), Structure and formation of the continental tectosphere, *J. Petrol.*, 11–37, Special Lithosphere Issue.

Kaminski, E., and C. Jaupart (2000), Lithosphere structure beneath the Phanerozoic intracratonic basins of North America, *Earth Planet. Sci. Lett.*, *178*, 139–149.

Katsura, T. (1995), Thermal diffusivity of olivine under upper mantle conditions, *Geophys. J. Int.*, *122*, 63–69.

Korenaga, J. (2006), Archean geodynamics and the thermal evolution of the Earth, in *Archean Geodynamics and Environments*, vol. 164, edited by K. Benn, J. C. Mareschal, and K. C. Condie, pp. 7–32, AGU Geophysical Monographs.

Lenardic, A. (2006), Continental growth and the Archean paradox, in *Archean Geodynamics and Environments*, vol. 164, edited by K. C. C. K. Benn and J-C. Mareschal, pp. 33–45, AGU Geophysical Monographs.

Lenardic, A., L.-N. Moresi, A. Jellinek, and M. Manga (2005), Continental insulation, mantle cooling, and the surface area of oceans and continents, *Earth Planet. Sci. Lett.*, *234*, 317–333.

Mareschal, J. C., and C. Jaupart (2004), Variations of surface heat flow and lithospheric thermal structure beneath the North American craton, *Earth Planet. Sci. Lett.*, *223*, 65–77.

Mareschal, J. C., A. Nyblade, H. K. C. Perry, C. Jaupart, and G. Bienfait (2004), Heat flow and deep lithospheric thermal structure at Lac de Gras, Slave province, Canada, *Geophys. Res.*, *31*.

McLennan, S. M., and S. R. Taylor (1996), Heat flow and the chemical composition of continental crust, *J. Geol.*, *104*, 377–396.

Michaut, C., and C. Jaupart (2004), Nonequilibrium temperatures and cooling rates in thick continental lithosphere, *Geophys. Res. Lett.*, *31*, L24602, doi:10.1029/2004GL021092.

Nicolaysen, L. O., R. J. Hart, and N. H. Gale (1981), The Vredefort radioelement profile extended to supracrustal strata at Carletonville, with implications for continental heat flow, *J. Geophys. Res.*, *86*, 10,653–10,661.

Niu, F., A. Levander, C. M. Cooper, C. A. Lee, A. Lenardic, and D. E. James (2004), Seismic constraints on the depth and composition of the mantle keel beneath the Kaapvaal craton, *Earth Planet. Sci. Lett.*, *224*, 337–346.

Nyblade, A. A., H. N. Pollack, D. L. Jones, F. Podmore, and M. Mushayandebvu (1990), Terrestrial heat flow in East and southern Africa, *J. Geophys. Res.*, *95*, 17,371–17,384.

Pearson, D. G. (1999), The age of continental roots, *Lithos*, *48*, 171–194.

Phillips, D., J. W. Harris, and K. S. Viljoen (2004), Mineral chemistry and thermobarometry of inclusions from de Beers pool diamonds, Kimberley, South Africa, *Lithos*, *77*, 155–179.

Pinet, C., and C. Jaupart (1987), The vertical distribution of radiogenic heat production in the Precambrian crust of Norway and Sweden: Geothermal implications, *Geophys. Res. Lett.*, *14*, 260–263.

Priestley, K. (1999), Velocity structure of the continental upper mantle: Evidence from southern Africa, *Lithos*, *48*, 45–56.

Richardson, S. H., J. J. Gurney, A. J. Erlank, and J. W. Harris (1984), Origin of diamonds in old enriched mantle, *Nature*, *310*, 707–711.

Roy, R. F., A. E. Beck, and Y. S. Touloukian (1981), Thermophysical properties of rocks, in *Physical Properties of Rocks*, vol. 2, edited by W. J. Y. S. Touloukian and R. Roy, pp. 409–502, McGraw-Hill, New York.

Rudnick, R. L., and A. A. Nyblade (1999), The thickness and heat production of Archean lithosphere: Constraints from xenolith thermobarometry and surface heat flow, in *Mantle Petrology: Field Observations and High Pressure Experimentation: A Tribute to Francis R. (Joe) Boyd*, edited by C. M. B. Y. Fei and B.O. Mysen, pp. 3–12, The Geochemical Society.

Rudnick, R. L., W. F. McDonough, and R. O'Connell (1998), Thermal structure, thickness and composition of continental lithosphere, *Chem. Geol.*, *145*, 395–411.

Russell, J. K., and M. G. Kopylova (1999), A steady-state conductive geotherm for the North Central Slave, Canada: Inversion of petrological data from the Jericho kimberlite pipe, *J. Geophys. Res.*, *104*, 7089–7101.

Schärmeli, J. F. (1979), Identification of radiative thermal conductivity in olivine up to 25 kbar and 1500 k, in *Proceedings of the 6th AIRAPT Conference*, pp. 60–74, Springer, New York.

Schatz, G., and G. Simmons (1972), Thermal conductivity of Earth materials, *J. Geophys. Res.*, *77*, 6966–6983.

Schmitz, M., and S. Bowring (2003), Constraints on the thermal evolution of continental lithosphere from U-Pb accessory mineral thermochronometry of lower crustal xenoliths, southern Africa, *Contrib. Mineral. Petrol.*, *144*, 592–618.

Schubert, G., D. Stevenson, and P. Cassen (1980), Whole planet cooling and the radiogenic heat source contents of the Earth and Moon, *J. Geophys. Res.*, *85*, 2531–2538.

Silver, P. G., M. Fouch, S. Gao, and M. Schmitz (2004), Seismic anisotropy, mantle fabric and the magmatic evolution of Precambrian southern Africa, *S. Afr. J. Geol.*, *107*, 45–58.

Skinner, C. P. (1989), The petrology of peridotite xenoliths from the Finsch kimberlite, South Africa, *Trans. Geol. Soc. S. Afr.*, *92*, 197–206.

Smith, D. (1999), Temperatures and pressures of mineral equilibration in peridotite xenoliths: Review, discussion, and implications, in *Mantle Petrology: Field Observations and High Pressure Experimentation: A Tribute to Francis R. (Joe) Boyd*., vol. 6, pp. 171–188, Geochemical Soc. Spec. Publ.

Sudo, A., and Y. Tatsumi (1990), Phlogopite and K-amphibole in the upper mantle: Implication for magma genesis in the subduction zones, *Geophys. Res. Lett.*, *17*, 29–32.

Taylor, W. (1998), An experimental test of some geothermometer and geobarometer formulations for upper mantle peridotites with application to the thermobarometry of fertile lherzolite and garnet websterite, *Neues Jahrb. Mineral. Abh.*, *172*, 381–408.

Thompson, P. H., A. S. Judge, and T. J. Lewis (1995), Thermal parameters in rock units of the Winter Lake-Lac de Gras area, Central Slave province, Northwest Territories. Implications for diamond genesis, *Curr. Res.*, 125–135.

Xu, Y., T. J. Shankland, S. Linhardt, D. C. Rubie, F. Langenhorst, and K. Klasinki (2004), Thermal diffusivity and conductivity of olivine, wadsleyite and ringwoodite to 20 GPa and 1373 K, *Phys. Earth Planet. Inter.*, *143*, 321–336.

D. R. Bell, Department of Chemistry and Biochemistry, and School of Earth and Space Exploration, Arizona State University, P.O. Box 871404, Tempe, AZ 85287-1404, USA.

C. Jaupart, Laboratoire de Dynamique des Systemes Geologiques, Institut de Physique du Globe de Paris, 4, place Jussieu, 75005 Paris, France.

C. Michaut, Department of Geology and Geophysics, Yale University, P.O. Box 208-109, New Haven, CT 06520-8109, USA. (chloe.michaut@yale.edu)